Manipulation of unidirectional side scattering of light in transition metal dichalcogenide nanoresonators

Jing Du,[1,*] Wenrui Bao,[2,*] Ruiyang Zhang,[2] Shiyu Shen,[2] Lin Yue,[2] Qi Ding,[2] Peng Xie,[2] Xiaoyu Kuang,[1,2] Hong Zhang,[2,3] and Wei Wang[2,†]

[1]*Institute of Atomic and Molecular Physics, Sichuan University, Chengdu 610065, China*

[2]*College of Physics, Sichuan University, Chengdu 610064, China*

[3]*Key Laboratory of High Energy Density Physics and Technology of Ministry of Education, Sichuan University, Chengdu 610065, China*

(Received 21 October 2023; revised 6 January 2024; accepted 26 February 2024; published 19 March 2024)

All-dielectric optical nanoantennas from high-refractive-index materials are becoming a promising way for efficient manipulation of light at the nanoscale. Here we propose an all-dielectric nanostructure based on bulk transition metal dichalcogenides (TMDs) with very simple geometry, a single-element nanodisk with an off-centered hole sited on glass substrate. We demonstrate that such TMD-based nanostructures can be utilized as a high-performance controllable directional nanoantenna due to its aspect of high refractive index in visible range. Owing to the off-centered hole, scattering spectrum of the nanodisk presents an extra Mie resonance, which is dominated by electric and magnetic dipole of Mie resonance. The interference between them leads to a transverse Kerker effect with an efficient unidirectional sides scattering around the Mie resonance. Importantly, we further investigate the intrinsic coupling between the TMD excitons and Mie resonance, as well as the influence of the coupling on the unidirectional side scattering of the system. We show that unidirectional side scattering occurs for both newly formed polariton states as a direct consequence of self-hybridized exciton-Mie interaction. Their directivities are strongly dependent on the directional feature of the Mie resonance, which can be effectively controlled by size of the nanodisk and the position of off-centered hole. Our results may provide exciting possibility for efficient light manipulations and are expected to open new pathways for the design of novel nanophotonic devices.

DOI: 10.1103/PhysRevB.109.115426

I. INTRODUCTION

The manipulation and localization of light at the nanoscale are of great importance both for fundamental research and a myriad of applications in nanophotonics [1,2]. Optical nanoantennas offer unprecedented opportunities to control and guide light in the subwavelength regime, enabling the development of novel and compact photonic devices [3,4]. Particular attention has been devoted to plasmonic nanoantennas formed by metallic nanostructures with subwavelength features [5–8]. The excitation of localized surface plasmons can squeeze light into length scales far below the diffraction limit with a tightly confined electric field, which greatly enhances light-matter interactions.

Importantly, as an efficient light scatterer, a plasmonic nanoantenna can be used to direct the scattered light into specific directions through an appropriate structural design. Nanoantenna with controllable directionality are of great use and find a variety of applications, such as controlling fluorescent emission for sensing or high-efficiency photon sources [9–13], optimizing performance through coupling to integrated photonic waveguides [14–16], and facile self-referenced detectors [17], etc. Different kinds of plasmonic nanostructures have been developed to realize directional antennas. Examples include Yagi-Uda antenna [18], V-shaped nanoantenna [19], U-shaped split-ring resonator [20], and triangular plasmonic nanoparticle [21]. However, plasmonic nanostructures possess unavoidable intrinsic absorption losses, especially at optical frequencies, greatly limiting the performance efficiencies of the optical nanoantennas. Nevertheless, functionality of plasmonic nanoantennas is predominately governed by the electric dipole response, with very weak interactions with the magnetic component of light. This restriction further limits novel designs with more degrees of freedom.

High-refractive-index dielectric nanostructures, such as silicon, have emerged as a promising platform for efficient directional manipulation at the subwavelength scale [22–25]. In contrast to their plasmonic counterparts, dielectric nanoparticles support strong electric and magnetic Mie-type resonances in the optical frequency with nearly zero energy losses, offering diverse degree of freedom to control light radiation with high efficiency. For example, strong forward or backward scattering was experimentally demonstrated [22,26,27] by exciting the electric dipole (ED) and magnetic dipole (MD) Mie resonances inside the nanoparticle (Kerker effect) [28]. Using the interference between multipolar excitations of Mie resonances [29–31], unidirectional or bidirectional transverse scattering was achieved for optical routing (V-shaped nanoantenna) [32,33], position sensing [34,35], optical force (notched silicon nanosphere) [36], and wide-angle invisible dielectric metasurface [37].

*These authors contributed equally to this work.

†w.wang@scu.edu.cn

Recently, multilayer or bulk transition metal dichalcogenides (TMDs) are becoming an extremely attractive class of materials due to their high in-plane refractive indices, which are higher than the best high-index semiconductor materials, such as silicon or germanium. Due to the high dielectric properties with intrinsic exciton transitions, nanostructured multilayer TMD materials can support various types of well-defined and intense Mie resonances in the visible to near-infrared spectral range, which can be manipulated in more degrees of freedom. Such unique optical properies steer both fundamental studies and promising applications in nanophotonics, for example, absorption enhancement [38,39], enhanement of fluoresence [40–43], self-hybridized strong coupling between the exciton and an optical mode induced by bulk TMDs [44–47], and nonlinear optical effects [48].

However, unlike traditional Si-based nanostructures, the study of bulk TMDs as dielectric scatterers for light manipulation has received little attention, with only a few studies focusing on directional emissions of fundamental or nonlinearly generated harmonic waves using TMD-based metasurfaces [41,49,50] and Kerker scattering in a self-hybridized case [50]. To the best of our knowledge, we are not aware of previous in-depth discussions examining the use of bulk TMD materials as optical nanoantennas for controllable directionality.

In this work, we propose a TMD-based nanostructure with a very simple geometry, demonstrating its capability of being a high-performance dielectric controllable directional nanoantenna. We design a single-element nanodisk with an off-centered hole sited on glass substrate. Owing to the off-centered hole, the scattering spectrum of the nanodisk presents an extra Mie resonance, called "EMD" peak, which is dominated by the electric and magnetic dipoles of Mie resonance. The interference between them leads to unidirectional scattering around the EMD peak which can be readily controlled by the geometrical parameters of the nanodisk. Importantly, we further investigate the coupling between the TMD excitons and the Mie resonance, as well as the influence of coupling on the unidirectional side scattering of the system. We show that, under the condition of self-hybridized exciton-Mie interaction, unidirectional side scattering occurs for both newly formed polariton states. Their directivities are strongly dependent on the directional feature of the Mie resonance, which can be effectively controlled by the size of the nanodisk and the position of the off-centered hole. Our results may provide exciting possibilities for efficient light manipulations and are expected to open new pathways for the design of novel nanophotonic devices.

II. RESULTS AND DISCUSSION

A. Unidirectional side scattering

The proposed nanodisk consists of bulk WS_2 with an off-centered hole, as shown in Fig. 1(a). The radius and thickness of the WS_2 nanodisk are $R = 120$ nm and $h = 70$ nm, respectively. Meanwhile, the center of the hole, with a radius $r = 40$ nm, is positioned on negative y axis and midpoint of the radius R, i.e., 60 nm away from the center of the nanodisk. The WS_2 disk is situated on a glass substrate. In

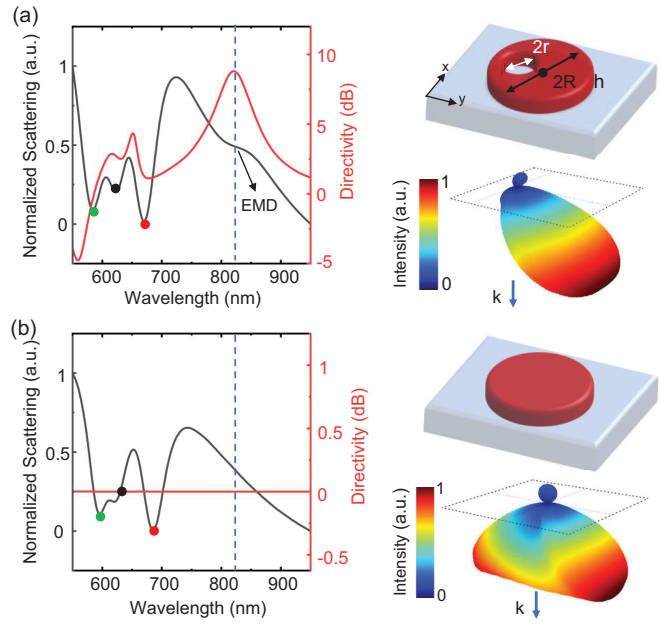

FIG. 1. Two distinct scenarios are illustrated: (a) a WS2 nanodisk concept with an off-centered hole on a glass substrate, illuminated by an x-polarized plane wave at normal incidence. The normalized scattering and directivity spectra from the nanodisk ($R = 120$ nm, $r = 40$ nm, and $h = 70$ nm) are presented on the left side, with a dashed blue line indicating the directivity peak and the three-dimensional (3D) pattern scattering corresponds to ~820 nm (indicated by the blue line) shown at bottom right. (b) Similar spectra for "pure" nanodisk under the same illumination and substrate conditions. The 3D scattering pattern at bottom right matches the blue line. Red and green dots mark two dips originated from the coupling between the A exciton and the anapole mode, while black dots denote the A exciton.

our design, the in-plane symmetry of the nanodisk has been intentionally broken. Under the illumination of linearly polarized light at normal incidence, both an electric dipole and a magnetic dipole are simultaneously excited. When these two modes are out of phase, their destructive interference results in unidirectional side scattering [31,36].

To study the scattering properties of the dielectric nanoantenna, we conducted simulations of the optical behavior of the system using the finite-difference time-domain (FDTD) method. For our simulations, we employed a total-field linearly polarized scattered-field source and perfect matching layer boundary conditions. The incident plane wave is polarized along the x direction and illuminates the nanodisk perpendicularly. The dielectric function of bulk WS2 is represented by the classical Lorenzian oscillator model, expressed as [44]

$$\epsilon = \epsilon_B + f_0 \frac{\omega_{ex}^2}{\omega_{ex}{}^2 - \omega^2 - i\gamma\omega_{ex}}, \tag{1}$$

where ϵ_B denotes background permittivity, f_0 represents the oscillator strength, ω_{ex} indicates resonance energy, and γ signifies the damping rate of the A-exciton resonance of WS_2. We adopt values $f_0 = 0.4$, $\omega_{ex} = 1.96$ eV, and $\gamma = 90$ meV, obtained from Ref. [44]. Initially,we computed the

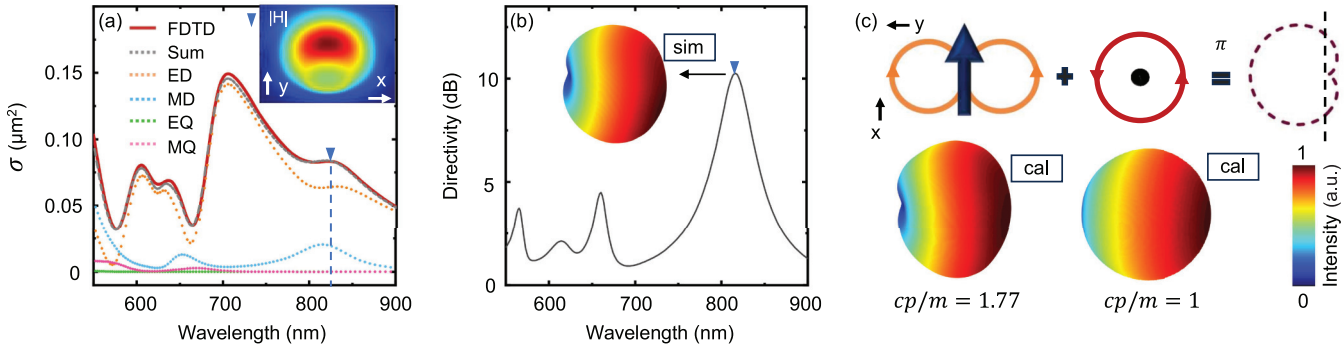

FIG. 2. (a) The multipole decomposition of the far-field scattering cross section is illustrated, and the WS_2 nanodisk is placed in vacuum. The contributions from EQ (dashed green) and MQ (dashed pink) are negligible. ED (dashed orange) and MD (dashed blue) mainly contribute to the scattering behavior of the nanodisk. The red line represents the sum of ED, MD, EQ, and MQ, while the dashed gray line is from scattering cross section simulated by finite-difference time-domain (FDTD). The dashed blue with a blue triangle is placed at ∼816 nm, consistent with panel (b). Magnetic near-field profile at ∼816 nm is shown at the top right. (b) The corresponding directivity spectrum. The directivity reaches its highest point at the wavelength corresponding to blue triangle, and its 3D scattering pattern is shown (left). (c) Superposition mechanism of the EMD pair at top. At different amplitude ratios ($cp/m = 1$ and $cp/m = 1.77$), 3D scattering patterns of theoretical calculation based on multipole decomposition are shown (bottom row).

far-field scattering spectrum and radiation patterns for the nanodisk with $R = 120$ nm, $r = 40$ nm, and $h = 70$ nm. In this context, the size of nanodisk (diameter and height) is optimized to make sure that the Mie resonance can occur close to the intrinsic excitonic frequency. Figure 1(a) depicts the far-field scattering behavior of the all-TMD nanodisk (black). Two prominent dips (marked by red and green dots) can be clearly seen in visible range, resulting from the strong coupling between the A excitons (indicated by the black dot) and the anapole generated by the nanodisk. In the near-infrared region, a broad "EMD" resonance occurs around 820 nm due to the in-plane symmetry breaking of the nanodisk by the presence of the off-centered hole. Note that the size of the off-centered hole is carefully optimized to ensure the EMD resonance exhibits strong-enough directional scattering. The physical origin of this mode will be discussed in more detail in subsequent sections. This "EMD" resonance completely disappears in absence of the hole, as demonstrated by the simulated scattering spectrum (black) of the "pure" nanodisk in Fig. 1(b). Interestingly, we observed unidirectional side scattering at the "EMD" resonance, depicted in the simulated three-dimensional (3D) scattering pattern (bottom right) in Fig. 1(a). Apparently, the nanodisk with a hole positioned at the negative y direction can predominantly direct free space radiation towards the y positive direction and vice versa. It should be noted that the negative and positive directions are defined in relation to the central point of the nanodisk (black dot). For the "pure" nanodisk, the scattered light into both directions of the y axis is equal, indicating a symmetry scattering behavior (bottom right), as shown in Fig. 1(b).

To quantitatively characterize the spectrally dependent directivity, we calculated directivity D as a function of wavelength for the nanodisk with and without the hole using the formula [2,19,32]:

$$D = 10\log_{10}\frac{\int_{-\delta}^{\delta}\int_{\theta_{\max}-\delta}^{\theta_{\max}+\delta} \mathrm{S}(\theta,\varphi)\sin\theta d\theta d\varphi}{\int_{\pi-\delta}^{\pi+\delta}\int_{\theta_{\max}-\delta}^{\theta_{\max}+\delta} \mathrm{S}(\theta,\varphi)\sin\theta d\theta d\varphi}, \tag{2}$$

where ϕ and θ represent the polar and azimuthal angles in spherical coordinates and S denotes Poynting vector. The calculation of S is referenced from Ref. [19]. For our calculation, we set $\theta_{\max}$ to 35° and δ to 10°. The calculated directivity (red curve) for the nanodisk with the hole, as shown in Fig. 1(a), reaches a maximum value of up to 10 at approximately 820 nm (indicated by dashed blue lines), coinciding with the position of the "EMD" peak. In contrast, the nanodisk without the hole exhibits no directivity across the entire wavelength range [red line in Fig. 1(b)]. This strongly suggests that the presence of the hole is responsible for the directional scattering of the nanoantenna.

B. Multipole decomposition

To gain further insight into the origin of the unidirectional scattering behavior of the WS2 nanodisk with an off-centered hole, we conduct a multipole decomposition of the far-field scattering from the nanoresonator, as illustrated in Fig. 2(a). The multipolar expansion method is an effective tool for understanding far-field spectral characteristics. The decomposition is conducted in the Cartesian coordinate system, and the approximated expressions of the multipole moments are given by [51,52]:

$$\begin{aligned}
p_\alpha &= -\frac{1}{i\omega}\left[\int J_\alpha d^3r + \frac{k^2}{10}\int[(\mathbf{r}\cdot\mathbf{J})r_\alpha - r^2 J_\alpha]d^3r\right]\\
m_\alpha &= \frac{1}{2}\int(\mathbf{r}\times\mathbf{J})_\alpha d^3r\\
Q_{\alpha\beta} &= -\frac{1}{2i\omega}\left[\int\{3(r_\alpha J_\beta + r_\beta J_\alpha) - 2(\mathbf{r}\cdot\mathbf{J})\delta_{\alpha\beta}\}d^3r\right.\\
&\quad + \frac{k^2}{14}\int\{4(r_\alpha r_\beta(\mathbf{r}\cdot\mathbf{J}) - 5r^2(r_\alpha J_\beta + r_\beta J_\alpha)\\
&\quad \left. + 2r^2(\mathbf{r}\cdot\mathbf{J})\delta_{\alpha\beta}\}d^3r\right]\\
M_{\alpha\beta} &= \int[r_\alpha(\mathbf{r}\times\mathbf{J})_\beta + r_\beta(\mathbf{r}\times\mathbf{J})_\alpha]d^3r\\
\mathbf{J} &= -i\omega\epsilon_0(n^2-1)\mathbf{E}(\mathbf{r}),
\end{aligned} \tag{3}$$

where ω is the frequency of light and r is the distance vector from the origin to the Cartesian coordinate point ($\alpha, \beta = x, y, z$). The symbols p, m, Q, and M represent the electric dipole moment p_α, the magnetic dipole moment m_α, the electric quadrupole moment $Q_{\alpha\beta}$, and the magnetic quadrupole moment $M_{\alpha\beta}$, respectively. The total scattering cross section can be calculated as

$$\sigma_{\text{sca}}^{\text{total}} = \frac{k^4}{6\pi\epsilon_0^2|\mathbf{E_0^2}|}\left[\sum\left(|\mathbf{p}|^2 + \left|\frac{\mathbf{m}}{c}\right|^2\right) + \frac{1}{120}\sum\left(|k\mathbf{Q}|^2 + \left|\frac{k\mathbf{M}}{c}\right|^2\right) + \cdots\right]. \quad (4)$$

Notably, this analysis is conducted without considering the presence of the glass substrate. Due to the low refractive index of glass, the electromagnetic fields are predominantly confined within the nanodisk. Therefore, this simplified analysis results in only minor spectral shifts.

The decomposition results in Fig. 2(a) clearly indicate that ED (orange) and MD (blue) modes are dominant, while contributions from electric quadrupole (EQ, green) and magnetic quadrupole (MQ, pink) are negligibly small. It is noteworthy that the structural parameters of the nanoantenna are identical to those shown in Fig. 1(a). The calculated decomposition results were further verified by our simulation. As shown in Fig. 2(a), the sum of all modes contributions (dashed gray) perfectly matches the total scattering cross section directly obtained from the FDTD simulation (solid red). Figure 2(b) (top left) displays the 3D scattering pattern at ∼816 nm (indicated by blue dashed line and blue triangle), clearly illustrating the unidirectional transverse scattering behavior along the positive y direction. Similarly, we calculate the directivity spectrum without the substrate, as depicted in Fig. 2(b), revealing that the highest value in the diagram nearly reaches up to 10.

Clearly, the ED and MD modes emerge at approximately ∼816 nm, with the directivity reaching its peak at the same wavelength. Remarkably, the strongest MD peak closely corresponds to this wavelength. The weak EMD resonance peak is dominated by ED and MD components. Simultaneously, the emergence of EDM peak originates from the presence of the off-centered hole, breaking the symmetry in the E-k plane. According to the generalized Kerker effect [28,30,31,35,53,54], the excitation of electric and magnetic dipoles can lead to unidirectional transverse scatterings. Figure 2(a) gives near-field plot of magnetic field in the xy plane at ∼816 nm (top right). For this strongest MD resonance peak at ∼816 nm, the magnetic near-field in the xy plane concentrates on the positive z direction, corresponding to an out-of-plane MD mode. As the incident light is polarized along the x axis, the ED mode must be in the plane. Consequently, the MD oscillates along the z axis, while the ED oscillates along the x axis. The interference between out-plane MD and in-plane ED results in transverse scattering [30]. In order to better understand this phenomenon, we assume that ED oscillates along x axis and MD oscillates along the z axis. The physical mechanism of EMD pair radiation can be visualized in Fig. 2(c) (top). In the E plane, the electric field lines of the electric dipoles exhibit a figure-8 shape, while the electric field lines of the magnetic dipoles are O shaped. The field lines with the same direction in the far field are enhanced, whereas those with the opposite direction are weakened [2]. When electric (p) and magnetic (m) dipole moments are met, $cp/m = 1$, with π phase difference, the scattering light will be radiated along the positive y axis. Consequently, the resulting radiation pattern is characterized by unidirectional transverse radiation, as shown in the 3D scattering pattern at the bottom right of Fig. 3(c).

It should be noted that the amplitudes of the ED and MD are not equal in our case due to inequality of p and m/c. As shown in Fig. 2(a), an apparent difference between the cross section at ED (dashed orange) and MD (dashed blue) resonance can be clearly seen. However, the difference between the corresponding resonant amplitude of ED and MD, which is proportional to dipole moment of ED and MD, is actually not that much. This is because the cross section is proportional to the square of dipole moment [Eq. (4)]. Therefore, unidirectional scattering still occurs although the resonant amplitudes of the electric and magnetic modes are not equal. In this sense, the system does not exhibit an ideal unidirectional scattering condition (the ratio of p to m/c, i.e., cp/m); instead, it demonstrates a degenerate unidirectional scattering with $cp/m = 1.77$ and a phase difference over 165°. The presence of degenerated unidirectional scattering is confirmed by our numerical simulation [inset of Fig. 2(b)] and theoretical calculation based on multipole decomposition [bottom row in Fig. 2(c)].

C. The coupling effect

In the above discussions, we have carefully designed the size of nanodisk and off-centered hole to tune the EMD resonance far away from the spectral region where the TMD exciton and nanodisk-induced Mie resonance occur [Figs. 1(a) and 1(b)]. The directional scattering at the EMD resonance can be easily analyzed without the influence of other resonances. However, it is well known that bulk TMD-based nanostructures, as high-refractive-index nanoresonators, are featured by the self-hybridization between excitons and the optical modes they support [44,47]. Such self-hybridizing systems greatly enrich the studies of light-matter interactions and may open a promising way of manipulating light at the nanoscale. Therefore, it is necessary to investigate the directionality effects of the present nanoantenna under self-hybridizing conditions. For this purpose, we brought the EMD mode in resonance with the TMD excitons by changing geometric parameters of the nanodisk and the off-centered hole.

We calculated a series of scattering spectra for different geometric configurations. Figure 3(a) shows scattering diagram of nanodisks as a function of radius R with fixed $r = 40$ nm and $h = 70$ nm. In contrast, Fig. 4(b) shows scattering diagram as a function of r with fixed $R = 85$ nm and $h = 70$ nm. In both cases, the parameters under variation can tune the EMD resonances across the A-exciton wavelength (marked by the dashed black lines), facilitating effective self-hybridization of exciton-EMD interactions. Clear mode splitting (dashed green and red lines) indicates the formation of hybridized exciton polaritons. The exciton-EMD coupling strength is approximately considered equivalent to that be-

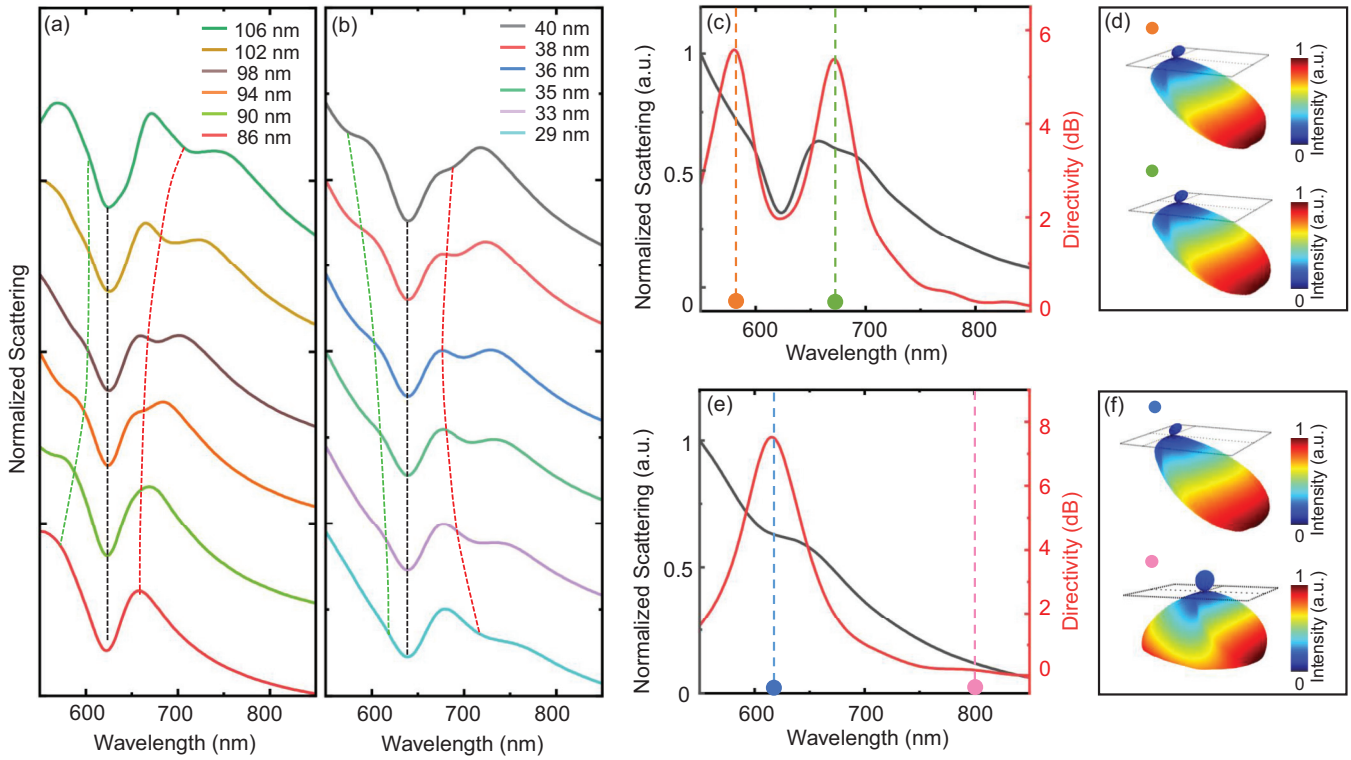

FIG. 3. Normalized scattering spectra of nanodisks with different sizes: The off-centered hole is positioned at a fixed distance $d = R/2$ away from the nanodisk's center. (a) The radius R of the nanodisk is varied and the hole's radius r of 40 nm is fixed, while (b) the radius r of the hole is varied and the nanodisk radius is fixed $R = 85$ nm. The red and black lines represent the normalized scattering and the corresponding directivity spectra of the nanodisk ($R = 90$ nm, $r = 35$ nm, and $H = 70$ nm), respectively, in case of (c) A exciton switched on or (d) A exciton switched off. [(e) and (f)] The 3D scattering pattern corresponding to the colored dots in Figs. 3(c) and 3(d) are shown.

tween the A-exciton and MD mode [depicted by the blue triangle in Fig. 2(a)]. In this sense, the coupling strength $\hbar\Omega$ evaluated by coupled oscillator model reaches 158 meV. Considering the damping rates of the exciton $2\hbar\gamma_{\text{exc}} = 90$ meV and MD mode $\hbar\gamma_M = 178$ meV, the inequation $\Omega > (\gamma_{\text{exc}} + \gamma_M)/2$ is satisfied, indicating that the system reaches a strong-coupling regime. Note that the Mie resonance induced by the nanodisk without the hole is not involved in the coupling for both cases. This is because the Mie resonance for the radius of nanodisk smaller than 100 nm occurs below 600 nm, which is far from the exciton resonance.

To explore the directional scattering property of the system under self-hybridizing conditions, we selected a nanodisk with $R = 90$ nm, $r = 35$ nm, and $h = 70$ nm, for which EMD mode closely resonates with the excitons. The simulated scattering spectrum (the black line) is plotted alongside the corresponding directivity (the red line) in Fig. 3(c). Two prominent peaks, with a maximum value up to 6, can be clearly seen in the directivity curve. Interestingly, the peaks of directivity occur precisely at the wavelengths of the polariton states (dashed green and orange lines). The directivity of the polariton states can be better visualized by plotting the 3D scattering pattern. As shown in Fig. 3(d), the scattered light is mostly directed towards the positive y direction at the wavelengths corresponding to the polariton states (green and orange dots). This strongly indicates that the existence of directionality results from the exciton-EMD coupling. This can be confirmed by simply "switching off" the excitonic transition. This can be achieved in our simulation by setting the oscillator strength of the exciton to be zero. The nanodisk became a pure high-refractive-index nanoresonator. In this case, only the EMD resonance (the dashed blue line) is observed in the scattering spectrum (the black line), with a single peak appearing at the same wavelength in the directivity curve (the red line), as shown in Fig. 3(e). The corresponding 3D scattering plot (at the top) is given in Fig. 3(f), along with one for another nonresonant wavelength (the dashed pink line), further confirming the high directionality of the EMD resonance in absence of self-hybridizing with excitons.

To further investigate the influence of exciton-EMD coupling on the scattering directionality in the self-hybridizing system, we further perform multipole decomposition on the scattering spectrum to analyze the contribution of the multipolar components to the directivity. The calculated results, as shown in Fig. 4(a), show four types of multipolar components. The ED (orange curve) and MD (blue curve) components are evidently dominant, while the electric quadrupole (EQ, green curve) and magnetic quadrupole (MQ, pink curve) are nearly zero. Importantly, both the ED and MD components exhibit a split profile, with their wavelengths perfectly aligned with those of the polariton states in the directivity curve (dashed gray). This means that the exciton-EMD coupling leads to polariton states that are half-exciton and half-EMD, and their directivity inherently arises from the directivity of EMD mode. To give a deeper insight into the directionality under self-hybridizing conditions, we introduce the rightward-

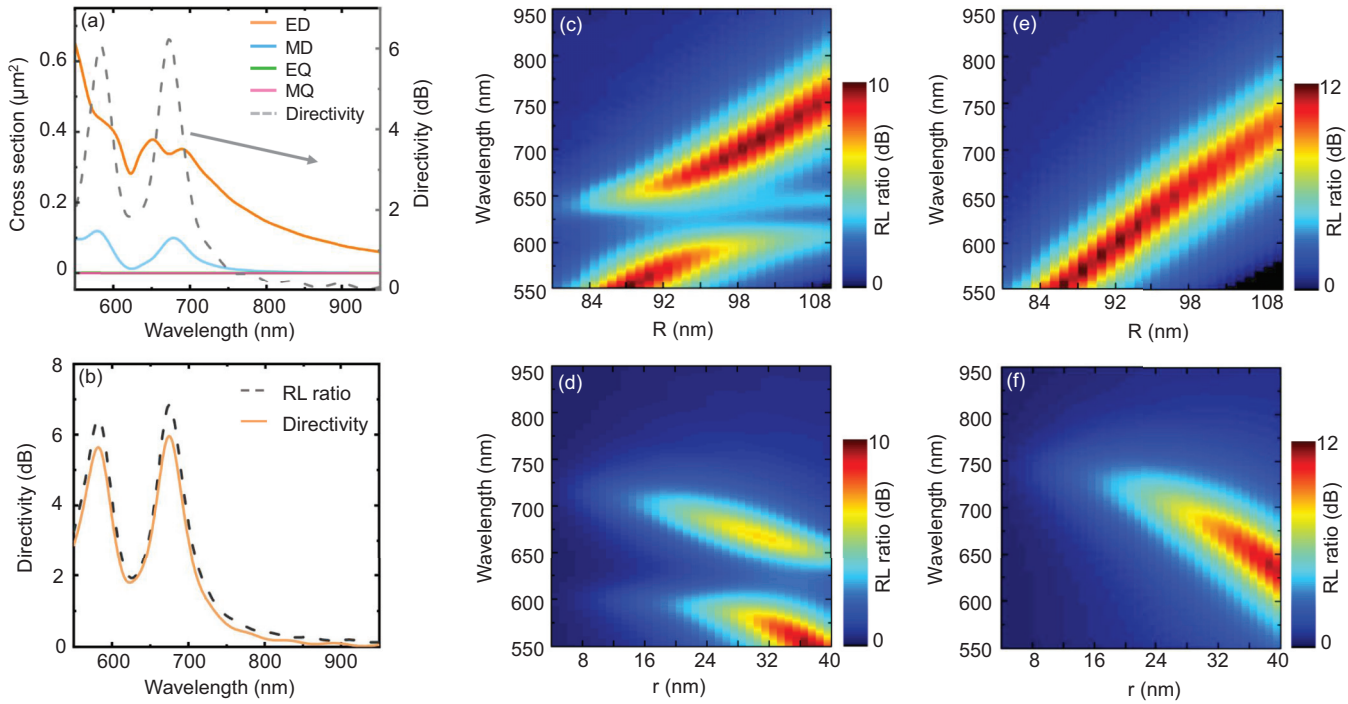

FIG. 4. (a) Multipole decomposition results are from the same dimensions as in Fig. 3(d) but in free space. Directivity spectrum is also depicted (dashed gray curve). The corresponding RL ratio is calculated as the ratio of the scattered intensity into the positive and negative y directions. (b) Simulated RL ratio (dashed black line) and directivity (yellow line) are shown for same nanodisk ($R = 85$ nm, $r = 28$ nm, and $h = 70$ nm) on glass substrate. To compare coupling with uncoupling effedts, RL ratio spectra are simulated [(c) and (d)] with A exciton switched on or [(e) and (f)] A exciton switched off. Simulated RL ratio spectra [(c) and (e)] as a function of R in color scale, [(d) and (f)] as a function of r in color scale. The color scale signifies the variations in the RL ratio for different R or r values.

to-leftward ratio (RL ratio), defined as the radio of power of the scattering light into a positive y direction to a negative y direction. The definition is similar to forward-to-backward ratio [26] and is calculated as

$$D_{\mathrm{RL}} = 10\log_{10}\frac{P_{yp}}{P_{yn}}, \tag{5}$$

where P_{yp} represents the power received in the positive y direction and P_{yn} represents the power received in the negative y direction. Figure 4(b) presents the RL ratio (dashed black) with the units of dB as a function of wavelength, along with the directivity spectrum, compared with RL ratio spectrum (solid orange) under the same geometrical conditions. We clearly see that these two curves match well with each other.

Using the definition given in Eq. (5), we further calculated the RL ratio as a function of the nanodisk radius (R) with fixed $r = 40$ nm [Fig. 4(c)]. Additionally, we calculated the RL ratio as a function of the hole radius (r) with fixed $R = 85$ nm, as shown in Fig. 4(d). The corresponding RL ratio for the uncoupled cases are given in Fig. 4(e) and Fig. 4(f), respectively. The results provide an intuitive picture on the relationship between the directivity and the geometry of the nanodisk. Figure 4(e) demonstrates the dependence of RL ratio at the EMD resonance on the radius of the disk. Increasing the radius R shifts the wavelength of directivity towards the red end of the spectrum. As a direct consequence of the exciton-EMD coupling, a clear anticrossing shape is visible in 2D maps of the RL ratio [Fig. 4(c)]. Therefore, tuning the radius R enables easy realization of directional scattering at the polariton resonances. For smaller radius with $R = 84$ nm, directional scattering occurs only at shorter wavelength below 550 nm. The directionality disappears around the excitonic resonance around 650 nm because the polariton is more exciton-like features. As the radius increases, the mixture of excitons and EMD states gives rise to two branches with equivalently high directionalities, which then becomes single-side directional scattering at longer wavelengths (again EMD-like) for larger radius because of the increased detuning of the exciton and EMD resonance. Similar scattering effects are observed in Fig. 4(d), where two branches of directional scattering are visible with varying radius of the hole. It is noteworthy that the directionality becomes weak at longer wavelengths for smaller radius r, which is due to the intrinsic weak directionality of the EMD mode for smaller radius r [Fig. 4(f)]. This is expected since a smaller hole will dramatically reduce the excitation efficiency of the EMD mode. Therefore, tuning the disk's radius with an optimized hole size is more favorable to obtain high-efficiency manipulation of directionality.

III. CONCLUSIONS

In summary, we have proposed a TMD-based all-dielectric nanoantenna with a simple configuration. We have demonstrated the capability of a single-element nanodisk as a high-performance controllable directional nanoantenna to efficient unidirectional light scattering. Due to its high refractive index and the existence of the off-centered hole, an extra Mie resonance dominated by electric and magnetic dipoles

can be excited. The interference between them leads to unidirectional scattering around the Mie resonance which can be readily controlled by the geometrical parameters of the nanodisk. Importantly, we further investigated the intrinsic coupling between the TMD excitons and Mie resonance, as well as the influence of the coupling on the unidirectional side scattering of the system. We have demonstrated the unidirectional side scattering occurring for both newly formed polariton states as a result of the self-hybridized exciton-Mie interaction. Their directivities are strongly dependent on the directional feature of the Mie resonance, which can be effectively controlled by size of the nanodisk and the off-centered hole.

ACKNOWLEDGMENTS

This work was supported by the National Natural Science Foundation of China (Grants No. 11974254 and No. 11974253) and Science Specialty Program of Sichuan University (Grant No. 2020SCUNL210).

[1] N. I. Zheludev, Nat. Mater. **7**, 420 (2008).
[2] N. Li, Y. Lai, S. H. Lam, H. Bai, L. Shao, and J. Wang, Adv. Opt. Mater. **9**, 2001081 (2021).
[3] L. Novotny and N. van Hulst, Nat. Photon. **5**, 83 (2011).
[4] S. Kruk and Y. Kivshar, ACS Photon. **4**, 2638 (2017).
[5] A. I. Kuznetsov, A. E. Miroshnichenko, M. L. Brongersma, Y. S. Kivshar, and B. Luk'yanchuk, Science **354**, aag2472 (2016).
[6] H. A. Atwater and A. Polman, Nat. Mater. **9**, 205 (2010).
[7] Z. Jiang, Y. Liu, and L. Wang, Opto-Electr. Sci. **1**, 210004 (2022).
[8] E.-M. You, Y. Chen, J. Yi, Z.-D. Meng, Q. Chen, S.-Y. Ding, H. Duan, M. Moskovits, and Z.-Q. Tian, Opto-Electr. Adv. **4**, 210076 (2021).
[9] D. Vercruysse, X. Z. Zheng, Y. Sonnefraud, N. Verellen, G. Di Martino, L. Lagae, G. A. E. Vandenbosch, V. V. Moshchalkov, S. A. Maier, and P. Van Dorpe, ACS Nano **8**, 8232 (2014).
[10] A. Krasnok, M. Caldarola, N. Bonod, and A. Alú, Adv. Opt. Mater. **6**, 1701094 (2018).
[11] Q. Deng, J. Chen, L. Long, B. Chen, H. Yu, and Z. Li, Opto-Electr. Adv. **5**, 210024 (2022).
[12] P. A. Dmitriev, E. Lassalle, L. Ding, Z. Y. Pan, D. C. J. Neo, V. Valuckas, R. Paniagua-Dominguez, J. K. W. Yang, H. V. Demir, and A. I. Kuznetsov, ACS Photon. **10**, 582 (2023).
[13] C. Li, J. Jang, T. Badloe, T. Yang, J. Kim, J. Kim, M. Nguyen, S. A. Maier, J. Rho, H. Ren, and I. Aharonovich, eLight **3**, 19 (2023).
[14] F. B. Arango, A. Kwadrin, and A. F. Koenderink, ACS Nano **6**, 10156 (2012).
[15] F. Peyskens, A. Dhakal, P. V. Dorpe, N. L. Thomas, and R. Baets, ACS Photon. **3**, 102 (2016).
[16] D. Vercruysse, P. Neutens, L. Lagae, N. Verellen, and P. V. Dorpe, ACS Photon. **4**, 1398 (2017).
[17] T. Shegai, P. Johansson, C. Langhammer, and M. Käll, Nano Lett. **12**, 2464 (2012).
[18] T. Kosako, Y. Kadoya, and H. F. Hofmann, Nat. Photon. **4**, 312 (2010).
[19] D. Vercruysse, Y. Sonnefraud, N. Verellen, F. B. Fuchs, G. Di Martino, L. Lagae, V. V. Moshchalkov, S. A. Maier, and P. Van Dorpe, Nano Lett. **13**, 3843 (2013).
[20] I. M. Hancu, A. G. Curto, M. Castro-López, M. Kuttge, and N. F. van Hulst, Nano Lett. **14**, 166 (2013).
[21] Y. Y. Tanaka and T. Shimura, Nano Lett. **17**, 3165 (2017).
[22] I. Staude, A. E. Miroshnichenko, M. Decker, N. T. Fofang, S. Liu, E. Gonzales, J. Dominguez, T. S. Luk, D. N. Neshev, I. Brener, and Y. Kivshar, ACS Nano **7**, 7824 (2013).
[23] J. Xu, Y. Wu, P. Zhang, Y. Wu, R. A. L. Vallée, S. Wu, and X. Liu, Adv. Opt. Mater. **9**, 2100112 (2021).
[24] Y. Fu, X. Wang, Z. Xing, W. Liu, and J. Cheng, Appl. Opt. **60**, 9205 (2021).
[25] H. Lee, A. Kecebas, F. Wang, L. Chang, S. K. Özdemir, and T. Gu, eLight **3**, 20 (2023).
[26] Y. H. Fu, A. I. Kuznetsov, A. E. Miroshnichenko, Y. F. Yu, and B. Luk'yanchuk, Nat. Commun. **4**, 1527 (2013).
[27] S. Person, M. Jain, Z. Lapin, J. J. Sáenz, G. Wicks, and L. Novotny, Nano Lett. **13**, 1806 (2013).
[28] M. Kerker, D. S. Wang, and C. L. Giles, J. Opt. Soc. Am. **73**, 765 (1983).
[29] R. Guo, E. Rusak, I. Staude, J. Dominguez, M. Decker, C. Rockstuhl, I. Brener, D. N. Neshev, and Y. S. Kivshar, ACS Photon. **3**, 349 (2016).
[30] A. Bag, M. Neugebauer, P. Woźniak, G. Leuchs, and P. Banzer, Phys. Rev. Lett. **121**, 193902 (2018).
[31] H. K. Shamkhi, K. V. Baryshnikova, A. Sayanskiy, P. Kapitanova, P. D. Terekhov, P. Belov, A. Karabchevsky, A. B. Evlyukhin, Y. Kivshar, and A. S. Shalin, Phys. Rev. Lett. **122**, 193905 (2019).
[32] J. Li, N. Verellen, D. Vercruysse, T. Bearda, L. Lagae, and P. Van Dorpe, Nano Lett. **16**, 4396 (2016).
[33] Y. Yu, J. Liu, Y. Yu, D. Qiao, Y. Li, and R. Salas-Montiel, Opt. Express **30**, 7918 (2022).
[34] M. Neugebauer, P. Woźniak, A. Bag, G. Leuchs, and P. Banzer, Nat. Commun. **7**, 11286 (2016).
[35] S. Nechayev, J. S. Eismann, M. Neugebauer, P. Woźniak, A. Bag, G. Leuchs, and P. Banzer, Phys. Rev. A **99**, 041801 (2019).
[36] A. Matsumori, H. Sugimoto, and M. Fujii, Laser Photon. Rev. **17**, 2300314 (2023).
[37] X. Zhang and A. L. Bradley, Phys. Rev. B **103**, 195419 (2021).
[38] A. Canales, O. Kotov, and T. O. Shegai, ACS Nano **17**, 3401 (2023).
[39] A. V. Prokhorov, A. V. Shesterikov, M. Y. Gubin, V. S. Volkov, and A. B. Evlyukhin, Phys. Rev. B **106**, 035412 (2022).
[40] J. Kern, A. Trügler, I. Niehues, J. Ewering, R. Schmidt, R. Schneider, S. Najmaei, A. George, J. Zhang, J. Lou, U. Hohenester, S. M. de Vasconcellos, and R. Bratschitsch, ACS Photon. **2**, 1260 (2015).
[41] N. Muhammad, Y. Chen, C. W. Qiu, and G. P. Wang, Nano Lett. **21**, 967 (2021).
[42] P. G. Zotev, Y. Wang, L. Sortino, T. S. Millard, N. Mullin, D. Conteduca, M. Shagar, A. Genco, J. K. Hobbs, T. F. Krauss, and A. I. Tartakovskii, ACS Nano **16**, 6493 (2022).

[43] B. R. Borodin, F. A. Benimetskiy, V. Y. Davydov, I. A. Eliseyev, A. N. Smirnov, D. A. Pidgayko, S. I. Lepeshov, A. A. Bogdanov, and P. A. Alekseev, Nanosc. Horiz. **8**, 396 (2023).

[44] R. Verre, D. G. Baranov, B. Munkhbat, J. Cuadra, M. Käll, and T. Shegai, Nat. Nanotechnol. **14**, 679 (2019).

[45] T. Weber, L. Kuhner, L. Sortino, A. B. Mhenni, N. P. Wilson, J. Kuhne, J. J. Finley, S. A. Maier, and A. Tittl, Nat. Mater. **22**, 970 (2023).

[46] M. Qin, J. Duan, S. Xiao, W. Liu, T. Yu, T. Wang, and Q. Liao, Phys. Rev. B **107**, 045417 (2023).

[47] P. Xie, Q. Ding, Z. Liang, S. Shen, L. Yue, H. Zhang, and W. Wang, Phys. Rev. B **107**, 075415 (2023).

[48] S. Busschaert, R. Reimann, M. Cavigelli, R. Khelifa, A. Jain, and L. Novotny, ACS Photon. **7**, 2482 (2020).

[49] M. Nauman, J. Yan, D. de Ceglia, M. Rahmani, K. Zangeneh Kamali, C. De Angelis, A. E. Miroshnichenko, Y. Lu, and D. N. Neshev, Nat. Commun. **12**, 5597 (2021).

[50] F. Shen, Y. Zhou, J. Ma, J. Zheng, J. Wang, Z. Chen, and J. Xu, Laser Photon. Rev. **18**, 2300584 (2024).

[51] A. B. Evlyukhin and B. N. Chichkov, Phys. Rev. B **100**, 125415 (2019).

[52] T. Hinamoto and M. Fujii, OSA Continuum **4**, 1640 (2021).

[53] W. Liu and Y. S. Kivshar, Opt. Express **26**, 13085 (2018).

[54] M. M. Bukharin, V. Y. Pecherkin, A. K. Ospanova, V. B. Il'in, L. M. Vasilyak, A. A. Basharin, and B. Luk-anchuk, Sci. Rep. **12**, 7997 (2022).